Post-fire Erosion and Recovery in Warrumbungle National Park – An Outlook

Qinggaozi Zhu[1], Xihua Yang[2], Anthony Clark[1]
1 Orange Agricultural Institute, New South Wales Department of Primary Industries, Australia
2 New South Wales Department of Planning, Industry and Environment, Parramatta, Australia

Key Points

- Soil loss from a single storm event can be up to 25 t ha^{-1}
- Average erosion declines due to groundcover recovery 1.5 years after bushfire
- The methodology is generic and readily applicable to other areas
- The high-resolution NDVI product and existing sensor network is vital for monitoring drinking water quality in the burnt area

Abstract

This paper describes a model based assessment methodology to track post bush fire erosion risk and recovery rates. It was developed following the 2013, a catastrophic bushfire ravaged Warrumbungle National Park (WNP) in New South Wales, which burnt almost 90% of the area. Subsequent storm events carried high levels of ash and particulate carbon into streams, which immediately affected water quality. In this study, post-fire erosion was modelled using the Revised Universal Soil Loss Equation (RUSLE) across WNP. Rainfall erosivity, was estimated by multi-source data fusion. Erosion rates were modelled from rainfall erosivity, groundcover, soil erodibility and landscape factors. Twelve soil plots were installed to observe soil loss and assess model performance. It was found that intensive rainfall events immediately after the bushfire increased erosion and sediment entering streams. A longer time gap between bushfire and significant rainfall event has less erosion risk due to opportunities for groundcover recovery when there are favourable seasonal conditions. Soil loss from a single storm event can be up to 25 t ha^{-1}, compared to the long-term average of 1.06 t ha^{-1} yr^{-1}. Despite differences in fire severity from soil plots, modelling and observations show consistent declines in average erosion due to widespread groundcover recovery after 1.5 years post fire. The methodology used here is generic and thus readily applicable to other areas where data are available. The methodology has potential to be applied to the large regions of NSW affected by the 2019-20 bushfires in particular regions like the Warragamba catchment where ongoing erosion and water quality risks remain. The modelling methodology described here can be strengthened by using information from existing sensor networks, which are essential for monitoring water quality monitoring in fire-affected areas by real-time tracking of salinity and nutrients, in conjunction with water sampling and lab analysis.

Keywords

post-fire erosion, water quality, bushfire recovery, catchment management

Introduction

Hillslope erosion after a wildfire often causes land degradation and adversely impacts the environment and water quality (Klik et al., 2015). Individual high-intensity rainstorms can account for appreciable quantities of postfire erosion. For example, in an early study in eucalypt forest near Sydney, Australia, Atkinson (1984) found that one rainfall event of 16.5 mm lasting 45 min caused the equivalent of a year's loss of soil. It is therefore critical to monitor, map, and disseminate both average and extreme erosion risks for catchments, given the predicted increase in climate variability and fire intensity in many parts of the world (Moody et al., 2013). Like cropping, wildfire removes the ground cover vagetation and results in insufficient cover to protect soils, which then become vulnerable to extreme erosive event. Hence, understanding the characteristics of the spatiotemporal distribution of wildfires and erosive rainfall events is critical for postfire recovery.

Rainfall and runoff erosivity (the 'R factor') as defined in the RUSLE (Renard et al., 1997) is the average annual value of the sum of all erosive events (EI_{30}) over a period of many years. For each storm event, the EI_{30} value is the product of storm energy, E, in MJ ha^{-1}, and peak 30-min rainfall intensity (I_{30}, mm hr^{-1}; Renard et al., 1997). Average monthly or annual rainfall erosivity has been assessed in several studies from long-term precipitation records and local rain gauges (Klik et al., 2015; Mello et al., 2013). There are few high-resolution studies on the spatial and temporal variation of daily EI_{30}, with the exception of Fischer et al. (2016) have estimated rainfall event erosivity by using radar data. However, there are few studies on the spatial and temporal variation of daily EI_{30} that use high temporal resolution products (e.g. weather radar) during a postfire recovery period, despite the key role of dynamic erosivity in hillslope erosion.

Severe wildfire and subsequent storm events increase erosion rates, change runoff generation, and potentially contaminate water supplies due to the increased flux of sediment, nutrients, and other water constituents. Severe wildfires reduce the resilience of soil to erosion by reducing vegetation and litter, reducing soil aggregate stability and increasing soil water repellence (Mataix-Solera et al., 2011), and have the potential to increase rainfall erosivity due to the loss of canopy. Consequently, hillslope erosion rates may vary according to the burn severity, vegetation recovery, and postfire rainfall events, though the relationship is not straightforward (Moody et al., 2013; Vieira et al., 2015). Therefore, quantitative and timely assessment of rainfall erosivity and hillslope erosion after wildfires during individual storm events is essential but remains a research challenge (Yin et al., 2015). The specific objectives of this research were to estimate daily EI_{30} and its spatial and temporal variation; assess the impact of events on daily EI_{30} and apply to near real-time hillslope erosion monitoring with further applications in post-fire erosion and water quality management.

Study area and data resource

The study area is approximately 450 km northwest of Sydney, centred on an area approximately 25 km west of Coonabarabran, and comprises Warrumbungle National Park (WNP) and the fire footprint of the 2013 wildfire (74,000 ha). The park ranges in elevation from 381 m to 1205 m above sea level. The climate is characterized by hot, usually humid summers and mild to cool winters.

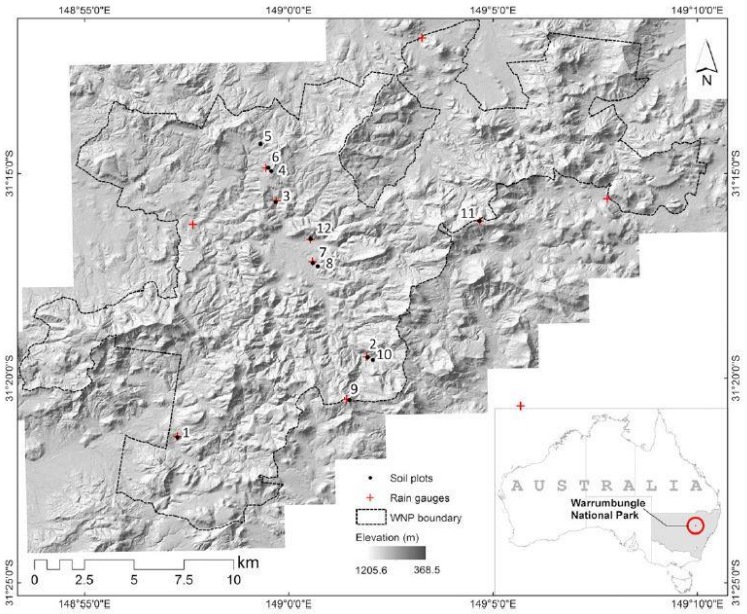

Figure 1. The Warrumbungle National Park (WNP) and the locations of soil plots (black dots) and rain gauges (red markers).

A severe wildfire ignited in WNP, New South Wales (NSW), Australia on 12 January 2013. Under the extreme fire weather, over 90% of the park was burnt, with 72% of the area categorized as high to

extreme burn severity. Fire severity was estimated from RapidEye images based on normalized burn ratio methods and categorized into four classes (0: unburnt; 1: low severity; 2: high severity; 3: extreme severity). Later, on 1 February 2013, an intense storm event (rainfall intensity > 50 mm h^{-1}) occurred, followed by several other storms where 100-150 mm of rain fell over the burnt area. These events led to extraordinary erosion and long-term landscape changes to the WNP.

Table 1. Site information of the 12 soil plots in WNP (top) and dataset used in this study

Data	Source	Description	Spatial (m)	Temporal	Period
ADS40	OEH	Aerial photograph	0.5 m	Once	Pre-2013
DEM	OEH, NASA	LiDAR, SRTM	1–30 m	Once	2013
Field	OEH	Soil, groundcover field data	Point	Quarterly	2014–16
Fire	OEH	Fire severity	30 m	Once	2013
Landsat	USGS	Landsat-8 imagery	30 m	16 days	2013–16
Groundcover	CSIRO	MODIS fractional cover Spectroradiometer	500 m	0.5 days	2000–16
Radar	BoM	Radar rainfall imagery	1000 m	10 min	2013–16
Rainfall	BoM, gauge	Gridded rainfall	5000 m	Daily	2013–16
Rapideye	AG German	High resolution satellite	5 m	5.5 days	2013–15
Soils	OEH, CSIRO	Soil properties and DSM	90 m	Once	2016/17

For this study, the weather radar at Namoi (Blackjack Mountain, -31.02° S, 150.19° E) at 10-min, 1 km were obtained from the Bureau of Meterology. Continuous radar images were obtained for the period from January to March 2013 immediately after the fire, and an extended period from January 2014 to June 2017 for on-going monitoring. A range of spatial and non-spatial datasets were collected for this study (Table 1). Field measurements include: (1) fractional groundcover measured at and around the 12 soil-plot sites based on the method described by Muir et al. (2011); (2) soil loss at the 12 soil plots; and (3) surface reflectance and temperature from various groundcover targets (soil, green vegetation, brown vegetation, litter and rocks) measured at satellite overpasses (normally at 0930 hours AEST) on clear days so that remote sensing-derived vegetation indices (such as normalised difference vegetation index, NDVI, and bare soil) can be validated. Accumulated sediment was collected during each field visit and sent to Yanco Natural Resources Laboratory, where the material was dried and weighed, and particle size classes and soil texture determined.

Method

Event-based EI_{30} estimation

To calculate the radar-derived rainfall accumulation, the raw radar reflectivity measurements (10-min, 1 km × 1 km) obtained from the Namoi weather radar station are firstly corrected by removing the effect of beam blocking. Then rainfall accumulation is converted from the corrected radar reflectivity through a Z-R relationship as below,

$$Z = 60\,R^{1.7} \tag{1}$$

where Z represents the reflectivity and R is the rain rate per pixel. Daily radar-derived rainfall estimations were adjusted against daily rain gauge observations through linear regression once the radar reflectivity was converted to rainfall accumulation and daily rainfall depth rate. The twelve tipping buckets gauges installed within WNP were used to calibrate the weather radar rainfall data.

The EI_{30} for a single storm event is the value of energy, E, in MJ ha^{-1}, multiplied by the peak 30-min rainfall intensity I_{30} (mm hr^{-1}). In this study, E is computed from the 10-min radar-based rainfall in 10-min intervals following Equation 2.

$$E = \sum_{r=1}^{N} e_r \Delta V_r \tag{2}$$

$$e_r = 0.29[1 - 0.72exp\,(-a\,\frac{\Delta V_r}{\Delta t_r})] \tag{3}$$

where $\Delta V_r/\Delta t_r$ is the rainfall intensity (mm hr^{-1}), while ΔV_r refers to rainfall amount during that particular period, Δt_r, N is the number of 10-minute intervals (e.g. N = 3 for 30-min), e_r (MJ ha^{-1} mm^{-1}) means unit kinetic energy, and a is an empirical coefficient. This form of the equation, including empirical coefficients, was based on the work of Kinnell (1981).

$$I_{30} = P_{30} \times 2 \tag{4}$$

The rainfall intensity for 30-min (mm hr^{-1}) intervals, I_{30} is calculated as where P_{30} is the maximum 30-

min rainfall depth (mm). It is multiplied by 2 to convert to an hourly scale. Peak rainfall amounts in 30-min intervals was extracted from radar images at every three 10-min intervals.

Event-based erosion modelling

Traditionally, the RUSLE has been applied to predicting the long-term average soil loss produced by rainfall erosion in many parts of the world (Wischmeier and Smith 1978; Renard et al. 1997). In the present study, the event-based erosion estimation was based on RUSLE with the R factor replaced by EI_{30} for the length of storm events.

$$A_i = (EI_{30})_i \times K_i \times LS \times C_i \times P,$$

where A_i is the predicted soil loss (Mg ha^{-1}) at event i, $(EI_{30})_i$ is EI_{30} (MJ mm ha^{-1} h^{-1}) for the storm event, K_i is the soil erodibility factor (Mg ha h ha^{-1} MJ^{-1} mm^{-1}) at that time, LS is the slope and steepness factor (unitless), Ci is the cover and management (C) factor (unitless) at the storm period (or monthly). The erosion control (P) factor (unitless) is not considered in this work for national parks. C factor was estimated by MODIS fractional cover and Landsat-8 imagery, which was calibrated by spectrum observation in WNP. Landscape factor was calculated by elevation data from STRM (1-30m), K factor was estimated from verified SALIS and recent DSM products (Grundy et al. 2015) for soil depths at 0–5, 5–15, 15–30, 30–60 and 60–100 cm.

Model performance was measured by the coefficient of efficiency, E_c (Nash & Sutcliffe, 1970), which is commonly used to assess model performance in hydrology and soil sciences. The common coefficient of determination (R^2), root mean square error (RSME) and standard error of the mean (SEM) were also applied to assess model performances by comparing the plot values (e.g. gauged rainfall data) with the simulated values estimated by weather radar and the KE-I relationship.

Results

Bias correction and radar rainfall variation

After calibration against the gauges in WNP, time-series rainfall depth maps derived from the radar data were produced at hourly, daily and monthly intervals. The daily rainfall amounts were accumulations over the previous 24 hours to 9:00 am local time. The peak radar rainfall was estimated to be as high as 61.87 mm for 2 February 2013. Hotspot areas with large daily rainfall amounts coincided with areas of extreme burn severity (e.g. on 18, 19, 22 Feb and 5 Mar 2013). These calibrated rainfall data were subsequently used for EI_{30} calculations, and compared with observed soil loss from hillslope plots on a monthly time-step.

EI_{30} and its temporal and spatial variation

To examine seasonal variation, monthly EI_{30} values were accumulated from daily radar-derived EI_{30} values and compared against the monthly EI_{30} values calculated from the gauge sites and pluviograph data. Table 2 shows the similar seasonal variation in EI_{30} from all these different data sources.

Table 2. Seasonal variation of EI_{30} and storm event assessment on Feb 1, 2013

Seasonal EI_{30} (RUSLE)	July 2015–June 2016			July 2016–June 2017			20130201 12:30–13:30	Rain		EI_{30} (RUSLE)		EI_{30} (RUSLE2)	
	RG	Radar	Pluviograph	RG	Radar	Pluviograph		Pluviograph	Radar	Pluviograph	Radar	Pluviograph	Radar
Summer	42.49%	31.55%	38.12%	24.44%	29.43%	35.90%	Daily	91.62%	86.95%	99.89%	88.65%	99.87%	86.89%
Autumn	19.93%	23.18%	18.95%	33.46%	28.51%	38.46%	Monthly	50.50%	29.13%	80.67%	31.22%	79.45%	31.11%
Winter	12.00%	21.52%	7.15%	10.31%	11.55%	2.01%	Seasonal	10.94%	8.03%	53.75%	9.28%	56.26%	10.18%
Spring	25.58%	23.75%	35.78%	31.78%	30.50%	23.63%	Annually	5.91%	-	37.63%	-	35.23%	-
Summer & Autumn	62.42%	54.73%	57.07%	57.90%	57.94%	74.36%	Month/season	21.67%	27.56%	66.63%	29.72%	70.81%	32.73%
Spring & Summer	68.07%	55.29%	73.90%	56.23%	59.94%	59.53%	Season/annual	53.96%	-	70.01%	-	62.62%	-

The higher EI_{30} values appeared in summer (December, January & February), with the EI_{30} values in winter (June, July & August) significantly lower. These trends are reflected in all EI_{30} estimates from radar, gauges and pluviograph measurements. Event-based EI_{30} was largely consistent with the radar-derived rainfall; each peak EI_{30} value corresponds to the peak rainfall intensity. For any given time-step (e.g. daily, monthly), the predicted rainfall erosivity varied spatially across the park. The EI_{30} fluctuated in response to the radar-derived rainfall estimates.

Figure 2 shows the daily EI_{30} of storm events and their spatial variation over the monitoring period (January 2013 to June 2017). These maps can be used to identify potential high erosion risk areas during

storm events. For example, the daily EI_{30} variation on 4 March 2017 in Figure 2 refers to a daily EI_{30} value as high as 826.76 MJ mm ha^{-1} hr^{-1} for a single event.

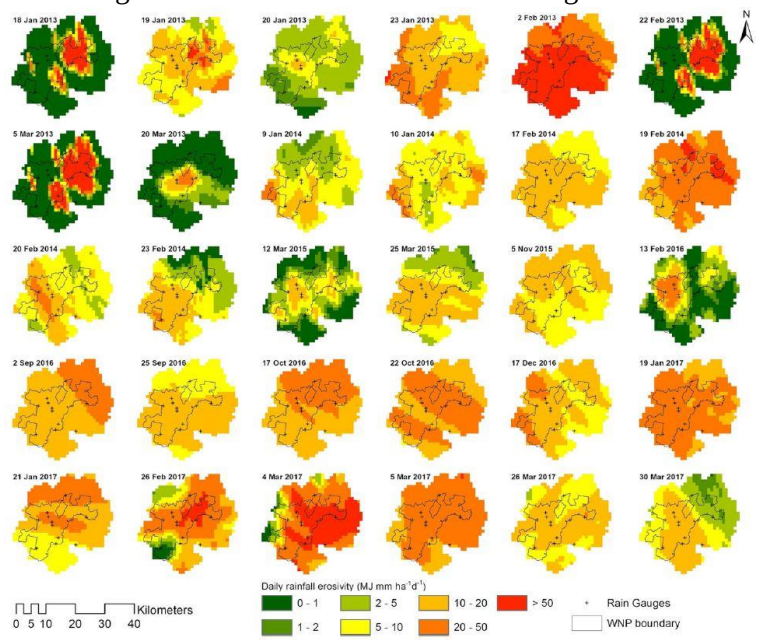

Figure 2. Time series EI_{30} maps and the spatial variations in the monitoring period from Jan 2013 to June 2017. ***EI_{30} distribution displayed is the actual annual estimation from the single storm event**

Impact of EI_{30} on erosion

The measured erosion during each field visit follows a similar seasonal pattern to the monthly EI_{30} in general (Figure 3), irrespective of which data source was applied (radar or gauge). Among the soil plots across the park, high erosivity was apparent at Site 1 and Site 11 as shown on Figure 4. Areas near these sites had experienced stronger storm events and flash flooding than most other soil plots. The higher cumulative EI_{30} values resulted in higher soil losses from the soil plots.

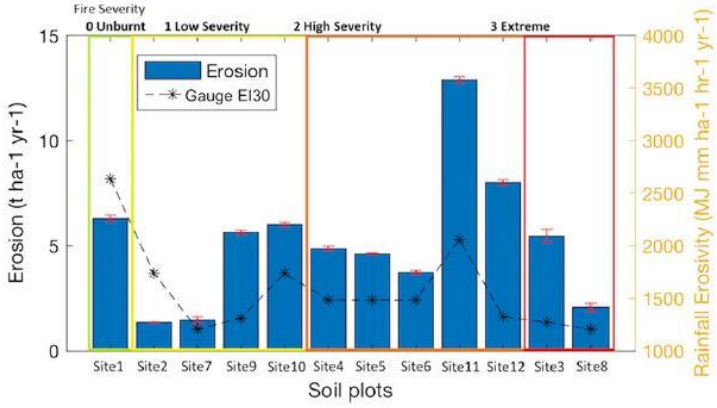

Figure 3. Spatial variation of rainfall erosivity and measured erosion between each soil plot. Soil plots grouped based on fire severity.

The relationship between the annual sum of EI_{30} and post-fire erosion was compared and assessed at the soil plot sites from July 2015 (Figure 3). The measured soil loss at each plot reflects the influence of EI_{30} but there is an obvious discrepancy between observed soil loss and EI_{30} values. For example, the highest erosion rates were measured at Site11; however, the corresponding EI_{30} was not the highest. Heavy rainfall occurred near Site2, but measured erosion rates from that soil plot were relatively low.

There exists a statistical difference of erosion rates according to the burn severity from the twelve measured erosion plots installed in 2014 (Table 3). Higher erosion occurred in extremely burnt areas within one year after the wildfire (Table 3), but such consistency became weaker in subsequent years (2016-17, Table 3) due to vegetation recovery and erosion control measures. Site 1 (unburnt) has higher

erosion rates compared to some burned areas (e.g. low severity class) due to its higher rainfall erosivity which is approximately two times higher than the low severity sites (2, 7, 9, 10). In the burn severity classification, there is essentially no difference between the 'unburnt' and 'low severity' classes as far as the groundcover is concerned. Therefore, other factors (EI_{30}, slopes) might be more influential in erosion than groundcover for these classes. This finding also suggests the need for an unambiguous classification as proposed by Vieira et al. (2015) who highlighted the incoherencies between existing burn severity classifications, and concluded that different burn severity does not evidence significant differences in post-fire runoff.

Table 3. The influence of EI_{30} (MJ mm ha^{-1} hr^{-1} yr^{-1}) on site erosion (t ha^{-1} yr^{-1}) at different fire severity classes

Fire severity	Sites	Average EI_{30} (MJ mm ha^{-1} hr^{-1} yr^{-1})	Average field erosion (n = 19) (t ha^{-1} yr^{-1})	Annual field erosion (t·ha^{-1}·yr^{-1})					
				2014–2015 (n = 8)		2015–2016 (n = 8)		2016–2017 (n = 3)	
				Mean	SEM	Mean	SEM	Mean	SEM
Unburnt	1	2777.00	1.00	1.59	-	0.46	-	0.87	-
Low severity	2, 7, 9, and 10	1620.85	0.60	1.07	0.25	0.27	0.08	0.48	0.21
High severity	4, 5, 6, 11, and 12	1657.55	1.03	1.60	0.58	0.63	0.14	0.59	0.22
Extreme severity	3 and 8	1354.13	1.12	2.19	0.32	0.42	0.19	0.13	0.06

Hillslope erosions were modelled from rainfall erosivity, groundcover factor, soil erodibility and landscape factor across WNP. Time-series hillslope erosion maps are shown in Figure 4. These maps show the spatial and temporal variation of hillslope erosion across WNP. For example, the erosion risk areas on 1 February 2013 were located in the eastern and southern parts of the Park, which agreed with our field observations. Soil loss from a single storm event comprises up to 25 t ha^{-1}, compared to a long-term average 1.06 t ha^{-1} yr^{-1}.

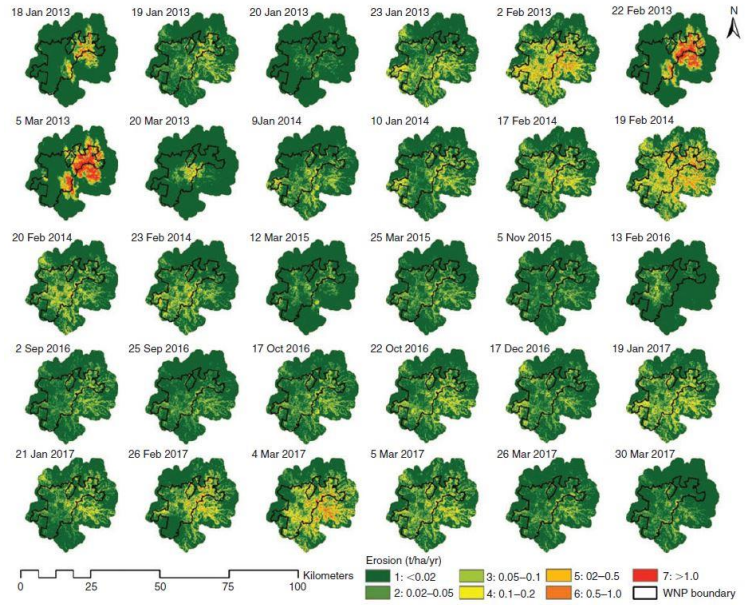

Figure 4. Daily soil loss in the fire-affected area based on radar-derived EI_{30} and RUSLE.

Discussion

Similar seasonal variation was apparent from the time-series of erosion measurements and monthly EI_{30}. Intensity, rather than the depth of rainfall event (Figure 2 and Table 2), highly affected the erosion rates. More soil loss was observed in summer when heavy rainstorms occurred, while less erosion was measured in the dry winters. In general, higher erosion rates were positively correlated with fire severity, however, relatively high erosion rates were also evident in some unburnt areas such as Site 1. This discrepancy is probably due to the vegetation recovery of burnt areas and the effects of other RUSLE factors such as soil, rainfall and topographic factors. For example, the slope steepness factor for Site 1 was measured as high as 0.3 with the highest rainfall erosivity among the twelve sites.

The average erosion from plots in extremely burnt areas decreased by about 94.1% from 2014 (2.19 t ha^{-1} yr^{-1}) to 0.13 t ha^{-1} yr^{-1} in 2017. In comparison, the erosion changes in low (1.07 t ha^{-1} yr^{-1} to 0.48 t ha^{-1} yr^{-1}) and high severity (1.60 t ha^{-1} yr^{-1} to 0.59 t ha^{-1} yr^{-1}) burn areas over three years gradually decreased by 55.0% and 63.1% respectively. One explanation for these differences is that the rapid vegetation recovery in high severity burn areas (Gordon et al., 2017) leads to a reduction of post-fire erosion rates. The groundcover in WNP has been generally increasing since the fire in early February 2013 and returned to near pre-burn levels within 1 year (Yang et al., 2018). There is an increasing trend from May 2014 (73%) to July 2017 (79%) according to the groundcover measurements, although the groundcover varies seasonally. Gordon et al. (2017) observed strong positive associations between *Acacia* species in WNP and total mid-story vegetation cover and fire severity. Results from this study also showed that the groundcover had recovered 1-1.5 years after the fire and the level of groundcover has continued to gradually improve since (to July 2017). The enhanced post-fire erosion is not directly and solely a result of fire severity, but it also related to a combination of the spatial distribution of rainfall and other erosion factors (e.g. groundcover and soil properties). This was further complicated by changes in these factors on different time scales (Moody et al., 2013). The time between the bushfire and significant rainfall event(s) plays an important role in post-fire erosion. Thus, mapping the burn severity, and not just the fire footprint, combined with radar-based event EI_{30} provides high spatio-temporal resolution information in relation to fire regime management.

RUSLE was originally designed to predict average annual soil loss. As such these models have limitations in predicting hillslope erosion for a particular storm event. However, some alternative process-based models are extremely sensitive to parameter estimations and those predictions are often poor while RUSLE requires low data inputs, is robust and has widely been used across the world. It is possible to estimate daily (or storm event-based) soil loss with time-series EI_{30} at a sub-daily scale as discussed above or the product of the runoff ratio (Q_R) and EI_{30} index (Kinnell, 2014) given the fact that soil erodibility and topographic factors are stable and groundcover factor changes seasonally (Yang et al., 2018).

Prediction of event-based EI_{30} will be increasingly important due to the higher likelihood of intense storm events under climate change. The current climate change projections predict that the region is trending towards an increased risk of wildfire due to warmer and drier conditions and higher frequencies of extreme weather such as storm events (Nyman et al., 2011). The methodology has potential to be applied to the large regions of NSW affected by the 2019-20 bushfires in particular regions like the Warragamba catchment where ongoing erosion and water quality risks remain.

Conclusions and future work

In this study, post-fire erosion was modelled using the RUSLE across WNP. Rainfall erosivity, one of the parameters in RUSLE, was estimated by multi-source data fusion including BoM weather radar, gridded rainfall and rain-gauge observation. Erosion rates were modelled from rainfall erosivity, groundcover factor, soil erodibility and landscape factor across WNP. Field measurements were conducted seasonally over a 5-year period after the bushfire (2013-2017) to assess the model accuracy.

It was found that intensive rainfall events immediately after the bushfire increased erosion and sediment entering rivers and streams. Intensity, rather than the depth of rainfall event, highly affected the erosion rates. The time between the bushfire and significant rainfall event(s) play an important role in post-fire erosion, where a longer time gap has less erosion risk due to opportunities for groundcover recovery when there are favourable seasonal conditions. Soil loss from a single storm event was modelling up to 25 t ha^{-1}, compared to a long-term average annual soil loss of 1.06 t ha^{-1} yr^{-1}. Despite differences in fire severity across WNP and soil plots, modelling and observations show declines in annual average erosion due to widespread groundcover recovery 1.5 years after the bushfire. The methodology developed in this study is generic and thus readily applicable to other areas where data are available. Management outcomes from the research included installation of erosion control works, redesign of access and monitoring of key mass movement hazard areas.

Future work will potentially include, but is not limited to, post-fire recovery at catchment level (e.g. usage of Landsat8 NDVI imagery and weather radar) and drinking water quality modelling for the mega-fire in summer 2019-20 in particular regions like the Warragamba catchment where ongoing erosion and water quality risks remain. It is highly important to establish an effective water quality monitoring program to minimise the impacts of bushfire. The modelling methodology described here can be strengthened by using information from existing sensor networks, which are essential for monitoring water quality monitoring in fire-affected areas by real-time tracking of salinity and nutrients, in conjunction with water sampling and lab analysis.

Acknowledgments

We thank the New South Wales Department of Planning, Industries and Environment (formally OEH) for providing funding and data for the WNP fire recovery research project and our subproject on Soil and Water. The BoM provided radar rainfall data. Many staff in the NSW National Park and Wildlife Services, Colleagues in Soil and Water, Fire Behavior, Vegetation and Fauna teams provided useful discussion, working on fieldtrip and advice to our sub-project. Colleagues in DRNSW, Dr Jennifer Wurtzel and Kim Broadfoot kindly reviewed and improved the paper.

References

Angulo-Martínez, M., Beguería, S., & Kyselý, J. (2016). Use of disdrometer data to evaluate the relationship of rainfall kinetic energy and intensity (KE-I). *Science of the Total Environment, 568*, 83-94. https://doi.org/10.1016/j.scitotenv.2016.05.223

Atkinson, G. (1984). Erosion damage following bushfires. *Journal of Soil Conservation New South Wales (Australia)*. http://escholarship.library.usyd.edu.au/journals/index.php/LIN

Fischer, F., Hauck, J., Brandhuber, R., Weigl, E., Maier, H., & Auerswald, K. (2016). Spatio-temporal variability of erosivity estimated from highly resolved and adjusted radar rain data (RADOLAN). *Agricultural and Forest Meteorology, 223*, 72-80. https://doi.org/10.1016/j.agrformet.2016.03.024

Foster, G., Yoder, D., Weesies, G., McCool, D., McGregor, K., & Bingner, R. (2003). RUSLE 2.0 user's guide. *USDA-Agricultural Research Service, Washington, DC*. https://www.tucson.ars.ag.gov/unit/Publications/PDFfiles/1117.pdf

Gordon, C. E., Price, O. F., Tasker, E. M., & Denham, A. J. (2017). Acacia shrubs respond positively to high severity wildfire: Implications for conservation and fuel hazard management. *Science of the Total Environment, 575*, 858-868. https://doi.org/10.1016/j.scitotenv.2016.09.129

Kinnell, P. (1981). Rainfall intensity-kinetic energy relationships for soil loss prediction. *Soil Science Society of America Journal, 45*(1), 153-155. https:// doi.org/10.2136/sssaj1981.03615995004500010033x

Kinnell, P. (2014). Modelling event soil losses using the $Q_R EI_{30}$ index within RUSLE2. *Hydrological Processes, 28*(5), 2761-2771. https://doi.org/10.1002/hyp.9790

Klik, A., Haas, K., Dvorackova, A., & Fuller, I. C. (2015). Spatial and temporal distribution of rainfall erosivity in New Zealand. *Soil Research, 53*(7), 815-825. https://doi.org/10.1071/SR14363

Löwe, R., Thorndahl, S., Mikkelsen, P. S., Rasmussen, M. R., & Madsen, H. (2014). Probabilistic online runoff forecasting for urban catchments using inputs from rain gauges as well as statically and dynamically adjusted weather radar. *Journal of Hydrology, 512*, 397-407. https://doi.org/10.1016/j.jhydrol.2014.03.027

Mataix-Solera, J., Cerdà, A., Arcenegui, V., Jordán, A., & Zavala, L. M. (2011). Fire effects on soil aggregation: a review. *Earth-Science Reviews*, 109(1-2), 44-60. https://doi.org/10.1016/j.earscirev.2011.08.002

Moody, J. A., Shakesby, R. A., Robichaud, P. R., Cannon, S. H., & Martin, D. A. (2013). Current research issues related to post-wildfire runoff and erosion processes. *Earth-Science Reviews*, 122, 10-37. https://doi.org/10.1016/j.earscirev.2013.03.004

Nash, J. E., & Sutcliffe, J. V. (1970). River flow forecasting through conceptual models part I—A discussion of principles. *Journal of Hydrology, 10*(3), 282-290. https://doi.org/10.1016/0022-1694(70)90255-6

Nyman, P., Sheridan, G. J., Smith, H. G., & Lane, P. N. (2011). Evidence of debris flow occurrence after wildfire in upland catchments of south-east Australia. *Geomorphology, 125*(3), 383-401. https://doi.org/10.1016/j.geomorph.2010.10.016

Renard, K. G., Foster, G. R., Weesies, G., McCool, D., & Yoder, D. (1997). *Predicting soil erosion by water: a guide to conservation planning with the Revised Universal Soil Loss Equation (RUSLE)* (Vol. 703): US Government Printing Office Washington, DC. https://naldc.nal.usda.gov/download/11126/PDF

Vieira, D.C.S., Fernández, C., Vega, J.A., Keizer, J.J. (2015). Does soil burn severity affect the post-fire runoff and interrill erosion response? A review based on meta-analysis of field rainfall simulation data. *Journal of Hydrology*, 523, 452-464. https://doi.org/10.1016/j.jhydrol.2015.01.071

Wischmeier, W. H., & Smith, D. D. (1978). *Predicting rainfall erosion losses-A guide to conservation planning*. https://www.cabdirect.org/cabdirect/abstract/19786726437

Wüest, M., Frei, C., Altenhoff, A., Hagen, M., Litschi, M., & Schär, C. (2010). A gridded hourly precipitation dataset for Switzerland using rain-gauge analysis and radar-based disaggregation. *International Journal of Climatology, 30*(12), 1764-1775. https://doi.org/10.1002/joc.2025

Yang, X., Zhu, Q., Tulan, M., McInnes-Clarke, S., Sun, L. & Zhang, X.P. (2018). Near real-time monitoring of post-fire hillslope erosion in a burnt national park after storm events. *International Journal of Wildland Fire*. https://doi.org/10.1071/WF18011 (Online early)

Yin, S.-q., Xie, Y., Liu, B., & Nearing, M. (2015). Rainfall erosivity estimation based on rainfall data collected over a range of temporal resolutions. *Hydrology and Earth System Sciences, 19*(10), 4113. https://doi.org/10.5194/hess-19-4113-2015